Semiconductor Physics, Quantum Electronics & Optoelectronics, 2026. V. 29, No 3. P. 302-310.

Semiconductor physics

Correlations between the dielectric properties, domain structure morphology and phase state of $Bi_{1-x}Sm_xFeO_3$ nanoparticles

O.S. Pylypchuk[1], V.O. Kolupaiev[1], V.V. Vainberg[1], V.N. Poroshin[1], I.V. Fesych[2,3], L.D. Demchenko[4,5], E.A. Eliseev[6*], and A.N. Morozovska[1]**

[1]*Institute of Physics, National Academy of Sciences of Ukraine, 46 Nauky Avenue, 03028 Kyiv, Ukraine*
[2]*Taras Shevchenko National University of Kyiv, 01030 Kyiv, Ukraine*
[3]*Donetsk Institute for Physics and Engineering named after O.O. Galkin, National Academy of Sciences of Ukraine*
[4]*Stockholm University, Department of Chemistry, Sweden*
[5]*Ye.O. Paton Institute of Materials Science and Welding, National Technical University of Ukraine "Igor Sikorsky Kyiv Polytechnic Institute", 37, Beresteisky Avenue, 03056 Kyiv, Ukraine,*
[6]*Frantsevich Institute for Problems in Materials Science, National Academy of Sciences of Ukraine, 3, Omeliana Pritsaka Str., 03142 Kyiv, Ukraine*
Corresponding author e-mail: eugene.a.eliseev@gmail.com[*], anna.n.morozovska@gmail.com[**]

Abstract. Nanoscale multiferroics are basic model objects for studying polar, magnetic, and magnetoelectric properties and mutual couplings. Bismuth-samarium ferrite ($Bi_{1-x}Sm_xFeO_3$) is a model orthoferrite, whose polar, magnetic and magnetoelectric properties have been studied for the bulk and thin film samples. The properties of $Bi_{1-x}Sm_xFeO_3$ nanoparticles have been much less studied, despite the nanoparticles can be used in a wide range of applications, such as energy storage, magnetic hyperthermia, and advanced nanoelectronics. In this work, we performed experimental measurements and analysis of the temperature dependence of the $Bi_{1-x}Sm_xFeO_3$ nanopowder dielectric properties. Calculations of the ferro-ionic coupling influence on the dielectric properties, domain structure morphology, and phase states are performed within the framework of the Ginzburg–Landau–Devonshire–Stephenson–Highland approach. Theoretical results explain the main trends of experimentally observed temperature dependences of the effective dielectric permittivity, which allows us to understand the correlations between the temperature behavior of dielectric properties, domain structure morphology, and phase state of $Bi_{1-x}Sm_xFeO_3$ nanoparticles.

Keywords: multiferroics, ferro-ionic coupling, dielectric properties, domain structure morphology, phase state.

https://doi.org/10.15407/spqeo29.03.302
PACS 75.85.+t, 77.22.-d

Manuscript received 11.03.26; revised version received 28.07.26; accepted for publication 16.09.26; published online 25.09.26.

1. Introduction

Nanoscale multiferroics, especially solid solutions of bismuth ferrite, both oxygen-deficient and doped with rare-earth ions of Sm, La, Pr, Eu [1–3], raise constant and significant scientific interest due to their interesting polar, magnetic and especially magnetoelectric properties [4, 5], which can be controlled by the size effects [6–8], deformation engineering [9, 10], as well as by the level of defects, such as oxygen vacancies [11] and/or rare earth dopants [12, 13]. However, in the practical implementation of such control, it is necessary to change the technological process of the synthesis of films and nanoparticles.

Modification of the surface state of ferroelectric perovskites is possible due to the surface electrochemical reaction in perovskites [14, 15]. As a result of electrochemical reactions at the surface, the so-called "chemical" polarization switching occurs [16–18]. The surface-driven electrochemical states can significantly improve the polar properties of thin films and nanoparticles of perovskite ferroelectrics, such as $PbTiO_3$ [14–18], $BaTiO_3$ [19, 20], antiferroelectrics $PbZrO_3$ [21], silicon-compatible ferroelectric-antiferroelectric oxides $Zr_xHf_{1-x}O_2$ [22, 23], chalcogenides $Sn_2P_2S_6$ [24, 25] and $CuInP_2S_6$ [26], and multiferroics $Bi_{1-x}Sm_xFeO_3$ [27, 28]. The main reason for this improvement is the surface adsorption (or desorption) of oxygen ions, which leads to appearance of mixed "ferro-ionic" states [29–31] in thin films and nanoparticles of the polar materials.

The properties of the rare-earth doped and/or co-doped $BiFeO_3$ nanoparticles [32, 33], fine-grained ceramics [34, 35], and nanocomposites [36] have been much less studied theoretically and experimentally compared to thin films, despite they can be used in a wide range of applications, such as energy storage [37], magnetic hyperthermia [38], and composite-based semiconductor devices.

In previous works [27, 28], we used the Ginzburg–Landau–Devonshire approach to calculate polar and dielectric properties of $Bi_{1-x}Sm_xFeO_3$ nanoparticles and construct their phase diagrams depending on the nanoparticle average size and samarium content "x". In this work, we perform experimental studies of the temperature dependence of the $Bi_{1-x}Sm_xFeO_3$ nanopowder dielectric permittivity. Calculations of the ferro-ionic coupling influence on the dielectric and polar properties are performed in the framework of combined Ginzburg–Landau–Devonshire (LGD) [27, 28] and Stephenson–Highland (SH) [14, 15] approaches. The main trends of experimental observations are explained by theoretical modeling, which allows us to establish correlations between the temperature behavior of dielectric properties, domain structure morphology, and phase state of $Bi_{1-x}Sm_xFeO_3$ nanoparticles.

2. Materials and methods

A series of nanopowder samples of $Bi_{1-x}Sm_xFeO_3$, where the Sm content "x" varies from 0 to 0.2 (shortly "BSFO"), were synthesized using the solution combustion method and then calcined for 5 hours at 750 °C to minimize the presence of residual water and hydroxyl groups. Preparation details are given in Ref. [27]. The obtained five samples were named as BFO, BSFO-005, BSFO-010, BSFO-015 and BSFO-020, respectively, where the numbers indicate the Sm content x = 0, 0.05, 0.1, 0.15, 0.2. According to the X-ray diffraction (XRD) data [27], the BFO sample contains 73% of the long-range ordered rhombohedral (*R*3*c*) $BiFeO_3$ phase, 16% of the orthorhombic (*Pbam*) $Bi_2Fe_4O_9$ phase, and 11% of the cubic (*I*23) $Bi_{25}FeO_{40}$ phase.

The Sm-doping very strongly increases the phase purity of the nanopowders. BSFO-005 contains 97% of $Bi_{0.95}Sm_{0.05}FeO_3$ in the *R*3c phase, 2% of $Bi_2Fe_4O_9$, and 1% of $Bi_{25}FeO_{40}$. BSFO-010 contains 99% of $Bi_{0.9}Sm_{0.1}FeO_3$ in the *R*3c phase and 1% of $Bi_{25}FeO_{40}$. BSFO-015 contains 7% and 92% of $Bi_{0.85}Sm_{0.15}FeO_3$ in the polar *R*3*c* and orthorhombic *Pbnm* phases, respectively, and 1% of $Bi_{25}FeO_{40}$. The BSFO-020 sample contains 99% of $Bi_{0.8}Sm_{0.2}FeO_3$ in the *Pbnm* phase and 1% of $Bi_{25}FeO_{40}$.

To measure the temperature dependences of the samples capacitance, the $Bi_{1-x}Sm_xFeO_3$ nanopowders were pressed in the polytetrafluoroethylene (PTFE) cells between two metallic plungers, which serve as electric contacts (see Fig. 1a). The samples in a cell have a disk shape with a 4 mm diameter and 0.2 mm thickness. The pressure to keep the samples resistance within reasonable limits was close to 2.5 MPa. The higher pressure applied to the samples does not result in noticeable changes in their electrophysical characteristics, and the measured values do not change after the pressure is removed.

The PTFE cell with plungers, providing sample compression, was placed inside the holder rod, which was connected to the RLC meter *via* a coaxial cable. The RLC meter UNI-T UT612 was used to measure the capacitance of the cells within the range 100…10^5 Hz. Heating of the samples was performed using the wire-wound nichrome heater connected to the controlled voltage source.

Typical transmission electron microscopy (TEM) images of the $Bi_{1-x}Sm_xFeO_3$ ($0 \le x \le 0.2$) nanoparticles are shown in Figs. 1b–1f. As seen from the images, the distribution of nanoparticle sizes is large enough (50…500 nm).

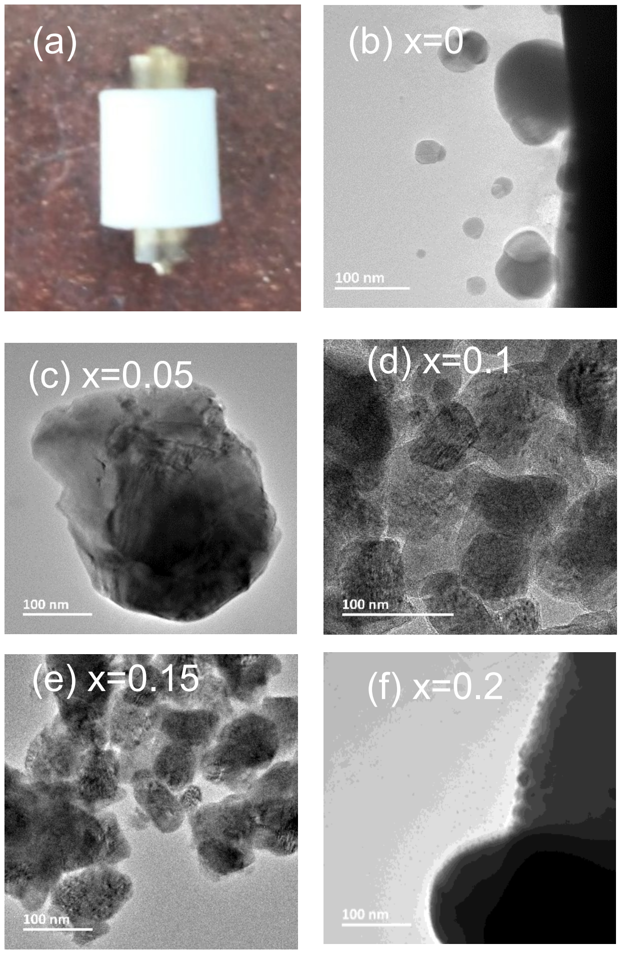

Fig. 1. (a) Schematic view of the cell with the sample. (b)–(f) Typical TEM images of the $Bi_{1-x}Sm_xFeO_3$ ($0 \le x \le 0.2$) nanoparticles.

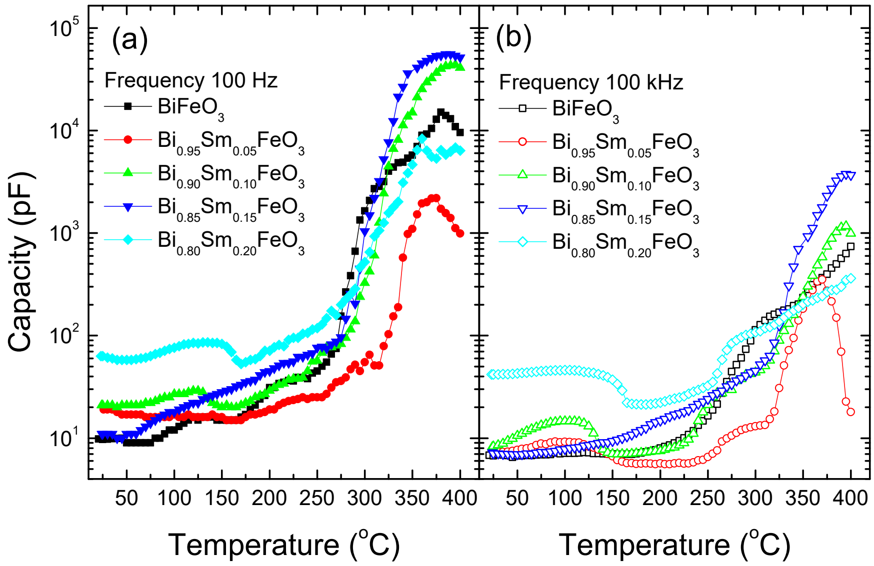

Fig. 2. Temperature dependences of the capacitance of pressed $Bi_{1-x}Sm_xFeO_3$ nanopowder tablets, measured at the frequencies 100 Hz (a) and 100 kHz (b).

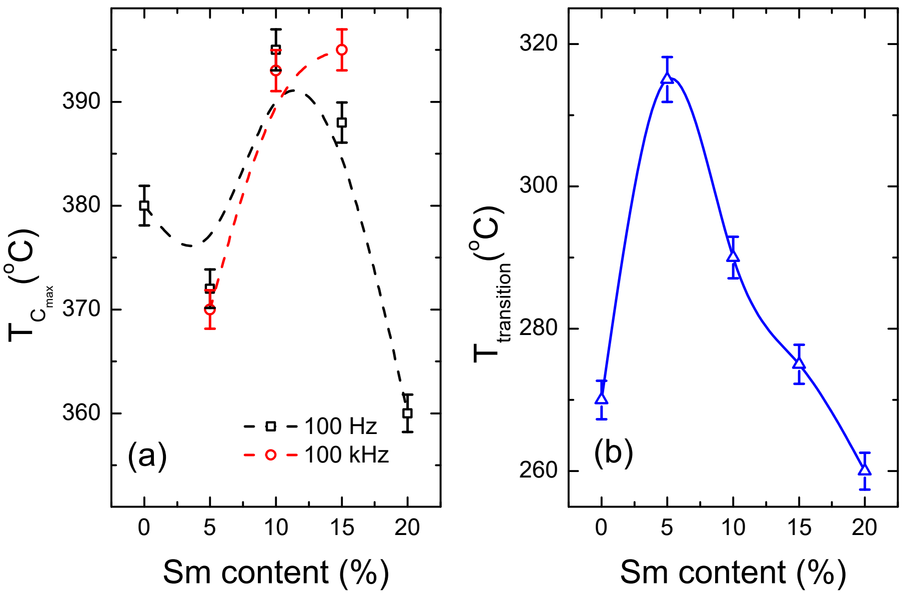

Fig. 3. (a) Dependence of the capacitance maximum temperature vs the Sm content in the $Bi_{1-x}Sm_xFeO_3$ nanopowders at 100 Hz and 100 kHz. (b) Dependence of the transition temperature between the low and high dielectric permittivity *vs* the Sm content in $Bi_{1-x}Sm_xFeO_3$ nanopowders at 100 Hz.

3. Experimental results and discussion

The temperature dependences of the capacitance of the studied samples with various Sm content were measured at the frequencies 100 Hz and 100 kHz within 20…400 °C. Typical results are shown in Fig. 2. The dependences have similar behavior for all Sm content "x" and consist of two characteristic parts. In the first part, corresponding to the temperature range from 20 °C to 250…300 °C, the capacitance, and consequently the effective dielectric permittivity of the nanopowders, are almost constant, manifesting only a very small increase in magnitude (from 10 to 60 pF) with growing temperature, which corresponds to the effective dielectric permittivity of several tens. At higher temperatures from 250…300 °C to 400 °C, the capacitance of all samples manifests rapid and strong growth with growing temperature, with the tendency to form a maximum at the highest temperature.

The dependence of the capacitance maximum temperature *vs* the Sm content is shown in Fig. 3a. As seen from Fig. 3a, the dependence is nonmonotonic for 100 Hz, and increases monotonically for 100 kHz.

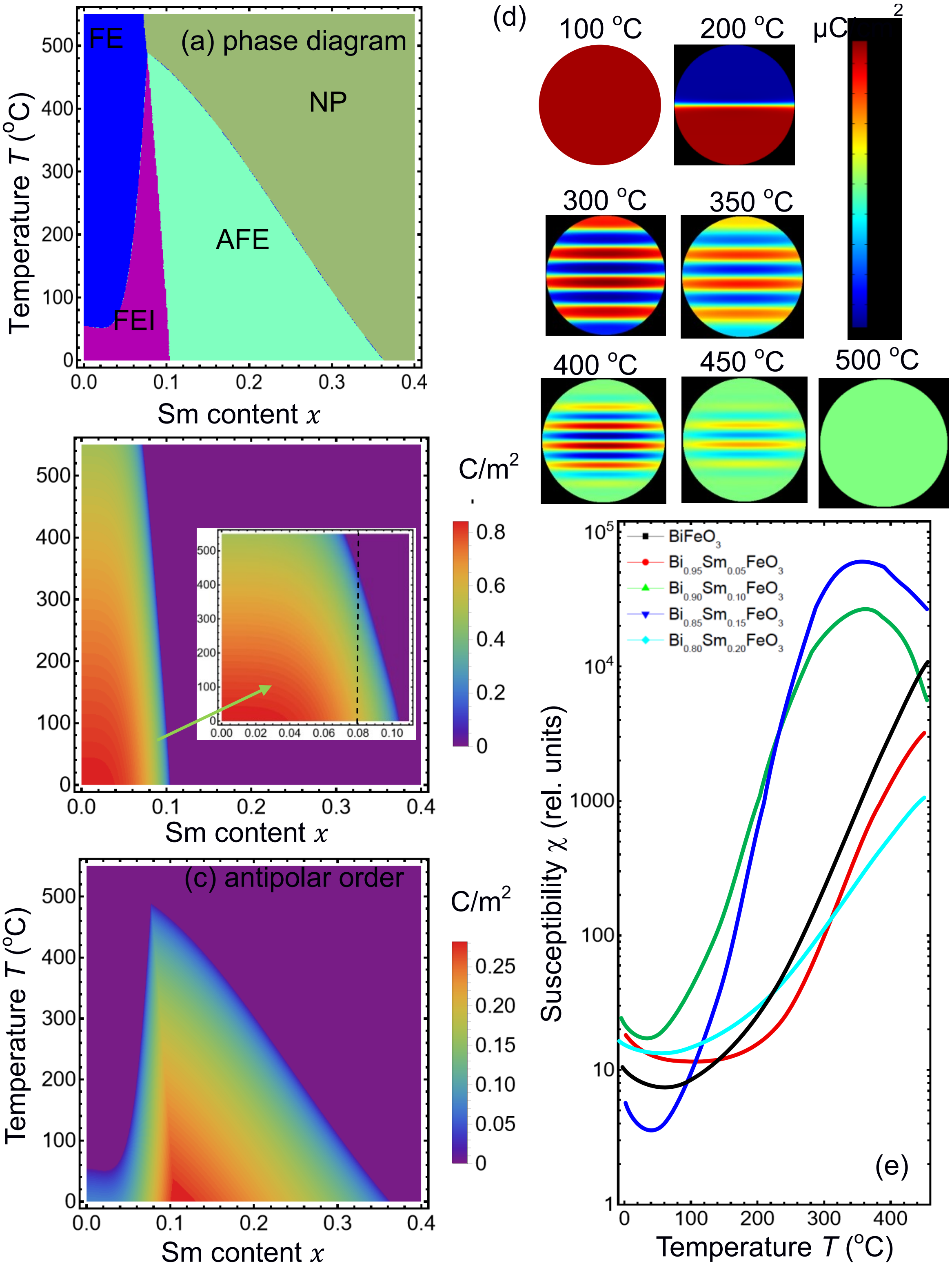

Fig. 4. The phase state (a), amplitudes of the spontaneous polar (b) and antipolar order (c) parameters as a function of Sm content x and temperature T calculated for the spherical $Bi_{1-x}Sm_xFeO_3$ nanoparticles with the size of 100 nm and effective surface screening length $\lambda = 1$ nm. (d) Temperature changes of the ferroelectric domain structure inside the 100-nm $Bi_{1-x}Sm_xFeO_3$ nanoparticle at x = 0.08. (e) Temperature dependences of the $Bi_{1-x}Sm_xFeO_3$ nanoparticles dielectric susceptibility (in relative units) calculated for growing Sm content x = 0 (black curve), 0.05 (red curve), 0.1 (green curve), 0.15 (blue curve) and 0.2 (cyan curves); the screening length $\lambda = 1$ nm, Maxwellian distribution of sizes with the most probable radius $R = 50$ nm and dispersion 100 nm.

Another important characteristic is the temperature of switching between the low and high dielectric permittivity regions. Fig. 3b shows the dependence of temperature at which the strong growth of the dielectric permittivity begins on the Sm content. It is also non-monotonic. At first, it sharply increases with the increase in Sm content from 0 to 5%, then it almost linearly decreases with Sm content increasing from 5 to 20%.

4. Theoretical modeling

As it was shown in Refs. [39, 40], the colossal dielectric constant of heterogeneous ferroelectric ceramics [41], nanopowders [42] and/or composites is usually caused by mesoscopic inhomogeneities in electrical conductivity (mainly between grains and grain boundaries), known as the effect of internal barrier layer capacitance (IBLC), as well as by inhomogeneous layers between electrodes and the sample, known as the effect of surface barrier layer capacitance (SBLC). The IBLC effect causes a colossal dielectric constant at low frequencies if the conductivity of the substance between grains is significantly lower than the conductivity of the grains. In this case, the percolation of components with low conductivity (*i.e.*, substances between ceramic grains) occurs and is described by the effective medium approach (EMA), discussed in Refs. [43, 44], as well as in the works of Petzelt *et al*. [45] and Rychetsky *et al*. [46].

The theoretical model of four cation sublattices, proposed in Ref. [47], allows the analytical description of cation displacement in the $Bi_{1-x}Sm_xFeO_3$ compounds, at that the Sm content "x" and the temperature T determine the stability of the long-range ordered rhombohedral ferroelectric (FE), mixed ferrielectric (FEI), antiferro-electric (AFE), and paraelectric/dielectric nonpolar (NP) orthorhombic phases. The free energy functional of the $Bi_{1-x}Sm_xFeO_3$ nanoparticles with ferro-ionic coupling was derived using the model of four sublattices, Landau–Ginsburg–Devonshire and Stephenson–Highland [14, 15] approaches in Ref. [27].

The phase state of the spherical $Bi_{1-x}Sm_xFeO_3$ nano-particles with a size of 100 nm as a function of Sm content x and temperature T is shown in Fig. 4a. The spontaneous polar and antipolar order parameters as a function of the Sm content x and temperature T are shown in Figs. 4b and 4c, respectively. The figures are calculated for the effective length of the surface screening $\lambda = 1$ nm, which originates from the ferro-ionic coupling with an adsorbed layer of ambient charges (*e.g.*, oxygen vacancies), and material parameters of $Bi_{1-x}Sm_xFeO_3$, listed in Ref. [27], except for the critical concentration of the antipolar order that is taken as $x_a = 0.35$ for better correlation with experimental results.

As seen from Figs. 4a–4c, the spontaneous polar order exists in the FE and FEI phases. The spontaneous antipolar order exists in the FEI and AFE phases, and gradually disappears approaching the FEI-FE boundary, as well as it disappears approaching the AFE-NP boundary. The antipolar order reaches maximal values at the FEI-AFE boundary. These results are also valid for the nanoparticles with the average radius $R = 50$ nm and negligibly small dispersion of sizes.

Typical temperature changes of the ferroelectric domain structure inside the 100-nm $Bi_{1-x}Sm_xFeO_3$ nanoparticle at x = 0.08 are shown in Fig. 4d. The single-domain state first transforms into the bi-domain with increase in temperature, then to the poly-domain, then domain stripes become low-contrast and vanish above the FE-NP phase transition temperature. Note that the temperature effects of the domain structure morphology become also significant near the FEI-AFE boundary [27].

Temperature dependences of the $Bi_{1-x}Sm_xFeO_3$ nanopowder dielectric susceptibility (in relative units) calculated for the growing Sm content x from 0 to 20% are shown in Fig. 4e by different curves. The dielectric susceptibility demonstrates characteristic features, such as a local minimum or maximum corresponding to the FE-FEI, FEI-AFE, or FE-NP phase transitions (compare different curves in Fig. 4e). The curves are smooth because they are averaged over a relatively wide size distribution of the nanoparticles (in agreement with the TEM analysis). The sharp variation corresponds to the second-order phase transition between the FEI and AFE phases (or FE-NP phases) in the ensemble of mono-dispersed nanoparticles. The temperature dependences of the $Bi_{1-x}Sm_xFeO_3$ nanopowder dielectric susceptibility, shown in Fig. 4e, correlate with the physical picture, shown in Fig. 2; however, there are significant differences, which we relate to the contribution of the Maxwell–Wagner mechanism, manifested as the IBLC and SBLC effects.

5. Conclusions

We performed experimental measurements and analysis of the temperature dependence of the $Bi_{1-x}Sm_xFeO_3$ nanopowders dielectric permittivity. The effective dielectric permittivity of the Sm-doped bismuth ferrite manifests interesting behavior with two characteristic temperature ranges, namely a slow increase from 20 °C to 250…300 °C followed by a sharp increase from 300 to 400 °C with the tendency to form a maximum. The magnitude of the dielectric permittivity in these ranges and the transition temperature between them depend non-monotonically on the Sm content.

Calculations of the ferro-ionic coupling influence on the dielectric properties, domain structure morphology, and phase states are performed in the framework of the Ginzburg–Landau–Devonshire–Stephenson–Highland approach. Theoretical results explain the main trends of experimentally observed temperature dependences of the effective dielectric permittivity, which allows us to understand the correlations between the temperature behavior of dielectric properties, domain structure morphology, and phase state of $Bi_{1-x}Sm_xFeO_3$ nanoparticles.

The chemically controlled dielectric permittivity is a key to desirable electrophysical properties, such as the magnetoelectric effect and electric conduction, for example, based on the Heywang model [48]. Thus, the results of the work can help to create ferroics with improved and/or controllable polar and dielectric properties, as well as expand the perspectives of their advanced applications in nanoelectronics and energy storage.

Acknowledgements

The work of O.S.P. and A.N.M. is funded by the National Research Foundation of Ukraine (project "Manyfold-degenerated metastable states of spontaneous polarization in nanoferroics: theory, experiment and perspectives for digital nanoelectronics", grant N 2023.03/0132). V.O.K., V.V.V. and V.N.P. acknowledge the Target Program of the National Academy of Sciences of Ukraine, Project No. 5.8/26-П "Energy-saving and environmentally friendly nanoscale ferroics for the development of sensorics, nanoelectronics and spintronics". The work of E.A.E. is funded by the National Research Foundation of Ukraine (project "Silicon-compatible ferroelectric nanocomposites for electronics and sensors", grant N 2023.03/0127). L.D. acknowledges support from the Knut and Alice Wallenberg Foundation (grant no. 2018.0237) for TEM research. I.V.F. is grateful to the II European Chemistry School for Ukrainians for providing a comprehensive overview of current trends in European chemical science.

References

1. Karpinsky D.V., Eliseev E.A., Xue F. *et al.* Thermodynamic potential and phase diagram for multiferroic bismuth ferrite ($BiFeO_3$). *npj Comput. Mater.* 2017. **3**. P. 20. https://doi.org/10.1038/s41524-017-0021-3.
2. Glinchuk M.D., Morozovska A.N., Karpinsky D.V., Silibin M.V. Anomalies of phase diagrams and physical properties of antiferrodistortive perovskite oxides. (Author review). *J. Alloys Compd.* 2019. **778**. P. 452–479. https://doi.org/10.1016/j.jallcom.2018.11.015.
3. Morozovska A.N., Karpinsky D.V., Alikin D.O. *et al.* A combined theoretical and experimental study of the phase coexistence and morphotropic boundaries in ferroelectric-antiferroelectric-antiferrodistortive multiferroics. *Acta Mater*. 2021. **212**. P. 116939. https://doi.org/10.1016/j.actamat.2021.116939.
4. Fiebig M. Revival of the magnetoelectric effect. *J. Phys. D: Appl. Phys*. 2005. **38**. P. R123. https://doi.org/10.1088/0022-3727/38/8/R01.
5. Fiebig M., Lottermoser T., Meier D., Trassin M. The evolution of multiferroics. *Nat. Rev. Mater*. 2016. **1**. P. 16046. https://doi.org/10.1038/natrevmats.2016.46.
6. Glinchuk M.D., Eliseev E.A., Morozovska A.N., Blinc R. Giant magnetoelectric effect induced by intrinsic surface stress in ferroic nanorods. *Phys. Rev. B*. 2008. **77**. P. 024106-1–11.
7. Maran R., Yasui S., Eliseev E. *et al.* Enhancement of dielectric properties in epitaxial bismuth ferrite – bismuth samarium ferrite superlattices. *Adv. Electron. Mater*. 2016. **2**, No 8. P. 1600170. https://doi.org/10.1002/aelm.201600170.
8. Sharma P., Morozovska A.N., Eliseev E.A. *et al.* Specific conductivity of a ferroelectric domain wall. *ACS Appl. Electron. Mater.* 2022. **4**. P. 2739–2746. https://pubs.acs.org/doi/10.1021/acsaelm.2c00261.
9. Sankara Rama Krishnan P.S., Morozovska A.N., Eliseev E.A. *et al.* Misfit strain driven cation interdiffusion across an epitaxial multiferroic thin film interface. *J. Appl. Phys*. 2014. **115**. P. 054103. https://doi.org/10.1063/1.4862556.
10. Zhou J., Huang H.-H., Kobayashi S. *et al.* An emergent quadruple phase ensemble in doped bismuth ferrite thin films through site and strain engineering. *Adv. Funct. Mater*. 2024. **34**. P. 2403410. https://doi.org/10.1002/adfm.202403410.
11. Morozovska A.N., Eliseev E.A., Sankara Rama Krishnan P.S. *et al.* Defect thermodynamics and kinetics in thin strained ferroelectric films: the interplay of possible mechanisms. *Phys. Rev. B*. 2014. **89**. P. 054102. https://doi.org/10.1103/PhysRevB.89.054102.
12. Lin T.K., Shen C.Y., Kao C.C. *et al.* Structural evolution, ferroelectric, and nanomechanical properties of $Bi_{1-x}Sm_xFeO_3$ films (x = 0.05–0.16) on glass substrates. *J. Alloys Compd*. 2019. **787**. P. 397. https://doi.org/10.1016/j.jallcom.2019.02.008.
13. Raghavan A., Pant R., Takeuchi I. *et al.* Evolution of ferroelectric properties in $Sm_xBi_{1-x}FeO_3$ *via* automated Piezoresponse Force Microscopy across combinatorial spread libraries. *ACS Nano*. 2024. **18**, No 37. P. 25591–25600. https://doi.org/10.1021/acsnano.4c06380.
14. Stephenson G.B., Highland M.J. Equilibrium and stability of polarization in ultrathin ferroelectric films with ionic surface compensation. *Phys. Rev. B*. 2011. **84**, No 6. P. 064107. https://doi.org/10.1103/PhysRevB.84.064107.
15. Highland M.J., Fister T.T., Fong D.D. *et al.* Equilibrium polarization of ultrathin $PbTiO_3$ with surface compensation controlled by oxygen partial pressure. *Phys. Rev. Lett*. 2011. **107**, No 18. P. 187602. https://doi.org/10.1103/PhysRevLett.107.187602.
16. Wang R.V., Fong D.D., Jiang F. *et al.* Reversible chemical switching of a ferroelectric film. *Phys. Rev. Lett*. 2009. **102**. P. 047601. https://doi.org/10.1103/PhysRevLett.102.047601.
17. Fong D.D., Kolpak A.M., Eastman J.A. *et al.* Stabilization of monodomain polarization in ultrathin $PbTiO_3$ films. *Phys. Rev. Lett*. 2006. **96**. P. 127601. https://doi.org/10.1103/PhysRevLett.96.127601.
18. Highland M.J., Fister T.T., Richard M.-I. *et al.* Polarization switching without domain formation at the intrinsic coercive field in ultrathin ferroelectric $PbTiO_3$. *Phys. Rev. Lett*. 2010. **105**. P. 167601. https://doi.org/10.1103/PhysRevLett.105.167601.
19. Yang S.M., Morozovska A.N., Kumar R. *et al.* Mixed electrochemical-ferroelectric states in nanoscale ferroelectrics. *Nat. Phys*. 2017. **13**. P. 812. https://doi.org/10.1038/nphys4103.
20. Morozovska A.N., Eliseev E.A., Biswas A. *et al.* Chemical control of polarization in thin strained

films of a multiaxial ferroelectric: Phase diagrams and polarization rotation. *Phys. Rev. B*. 2022. **105**. P. 094112. https://doi.org/10.1103/PhysRevB.105.094112.

21. Morozovska A.N., Eliseev E.A., Biswas A. *et al.* Effect of surface ionic screening on polarization reversal and phase diagrams in thin antiferroelectric films for information and energy storage. *Phys. Rev. Appl*. 2021. **16**. P. 044053. https://doi.org/10.1103/PhysRevApplied.16.044053.
22. Kelley K.P., Morozovska A.N., Eliseev E.A. *et al.* Ferroelectricity in hafnia controlled via surface electrochemical state. *Nat. Mater*. 2023. **22**. P. 1144. https://doi.org/10.1038/s41563-023-01619-9.
23. Eliseev E.A., Kalinin S.V., Morozovska A.N. Ferroionic states and domains morphology in $Hf_xZr_{1-x}O_2$ nanoparticles. *J. Appl. Phys.* 2025. **137**. P. 034103. https://doi.org/10.1063/5.0243067.
24. Morozovska A.N., Kalinin S.V., Yelisieiev M.E. *et al.* Dynamic control of ferroionic states in ferroelectric nanoparticles. *Acta Mater*. 2022. **237**. P. 118138. https://doi.org/10.1016/j.actamat.2022.118138.
25. Kalinin S.V., Eliseev E.A., Morozovska A.N. Adsorption of ions from aqueous solutions by ferroelectric nanoparticles. *Phys. Rev. Appl.* 2025. **23**. P. 014081. https://doi.org/10.1103/PhysRevApplied.23.014081.
26. Morozovska A.N., Kalinin S.V., Eliseev E.A. *et al.* Ferri-ionic coupling in $CuInP_2S_6$ nanoflakes: Polarization states and controllable negative capacitance. *Phys. Rev. Appl*. 2024. **22**. P. 034059. https://doi.org/10.1103/PhysRevApplied.22.034059.
27. Morozovska A.N., Eliseev E.A., Fesych I.V. *et al.* Reentrant polar phase induced by the ferro-ionic coupling in $Bi_{1-x}Sm_xFeO_3$ nanoparticles. *Phys. Rev. B*. 2024. **110**. P. 224110. https://doi.org/10.1103/PhysRevB.110.224110.
28. Pylypchuk O.S., Kolupaiev V.O., Fesych I.V. *et al.* Investigation of electrophysical properties, phase diagrams and charge carrier transfer in $Bi_{1-x}Sm_xFeO_3$. *Ukr. J. Phys*. 2025. **70**, No 10. P. 717. https://doi.org/10.15407/ujpe70.10.717.
29. Morozovska A.N., Eliseev E.A., Morozovsky N.V., Kalinin S.V. Ferroionic states in ferroelectric thin films. *Phys. Rev. B*. 2017. **95**. P. 195413. https://doi.org/10.1103/PhysRevB.95.195413.
30. Morozovska A.N., Eliseev E.A., Kurchak A.I. *et al.* Effect of surface ionic screening on polarization reversal scenario in ferroelectric thin films: crossover from ferroionic to antiferroionic states. *Phys. Rev. B*. 2017. **96**. P. 245405. https://doi.org/10.1103/PhysRevB.96.245405.
31. Highland M.J., Fister T.T., Richard M.-I. *et al.* Polarization switching without domain formation at the intrinsic coercive field in ultrathin ferroelectric $PbTiO_3$. *Phys. Rev. Lett.* 2010. **105**. P. 167601. https://doi.org/10.1103/PhysRevLett.105.167601.
32. Khist V.V., Eliseev E.A., Glinchuk M.D. *et al.* size effects of ferroelectric and magnetoelectric properties of semi-ellipsoidal bismuth ferrite nanoparticles. *J. Alloys Compd.* 2017. **714**. P. 303–310. https://doi.org/10.1016/j.jallcom.2017.04.201.
33. Eliseev E.A., Khist V.V., Fomichov Y.M. *et al.* Fixed volume effect on polar properties and phase diagrams of ferroelectric semi-ellipsoidal nanoparticles. *Eur. Phys. J. B*. 2018. **91**. P. 150. https://doi.org/10.1140/epjb/e2018-90133-6.
34. Morozovska A.N., Eliseev E.A., Glinchuk M.D. *et al.* Rotomagnetic coupling in fine-grained multiferroic $BiFeO_3$: theory and experiment. *Phys. Rev. B*. 2018. **97**. P. 134115. https://doi.org/10.1103/PhysRevB.97.134115.
35. Palaimiene E., Macutkevic J., Karpinsky D.V. *et al.* Dielectric investigations of polycrystalline samarium bismuth ferrite ceramic. *Appl. Phys. Lett*. 2015. **106**. P. 012906. https://doi.org/10.1063/1.4905344.
36. Karpinsky D.V., Fesenko O.M., Silibin M.V. *et al.* Ferromagnetic-like behavior of $Bi_{0.9}La_{0.1}FeO_3$-KBr nanocomposites. *Sci. Rep*. 2019. **9**, Art. number 10417. https://doi.org/10.1038/s41598-019-46834-0.
37. Bougoffa A., Benali E.M., Benali A. *et al.* Investigation of temperature and frequency dependence of the dielectric properties of multiferroic $(La_{0.8}Ca_{0.2})_{0.4}Bi_{0.6}FeO_3$ nanoparticles for energy storage application. *RSC Adv*. 2022. **12**, No 11. P. 6907–6917. https://doi.org/10.1039/d1ra08975g.
38. Papadopoulos K., Myrovali E., Karfaridis D. *et al.* Cation substitution and size confinement effects on structure, magnetism and magnetic hyperthermia of $BiFeO_3$-based multiferroic nanoparticles and hydrogels. *J. Alloys Compd*. 2023. **969**. P. 172337. https://doi.org/10.1016/j.jallcom.2023.172337.
39. Han H., Ghosh D., Jones J.L., Nino J.C. Colossal permittivity in microwave sintered barium titanate and effect of annealing on dielectric properties. *J. Am. Ceram. Soc.* 2013. **96**. P. 485. https://doi.org/10.1111/jace.12051.
40. Petzelt J., Nuzhnyy D., Bovtun V. *et al.* Broadband dielectric and conductivity spectroscopy of inhomogeneous and composite conductors. *phys. status solidi (a)*. 2013. **210**. P. 2259. https://doi.org/10.1002/pssa.201329288.
41. Pylypchuk O.S., Ivanchenko S.E., Yelisieiev M.Y. *et al.* Behavior of the dielectric and pyroelectric responses of ferroelectric fine-grained ceramics. *J. Am. Cer. Soc*. 2025. **108**. P. e20391. https://doi.org/10.1111/jace.20391.
42. Pylypchuk O.S., Vainberg V.V., Poroshin V.N. *et al.* A colossal dielectric response of $Hf_xZr_{1-x}O_2$ nanoparticles. *Phys. Rev. Mater*. 2025. **9**. P. 114412. https://doi.org/10.1103/y2pb-5g5w.
43. Saleem M., Butt M.S., Maqbool A. *et al.* Percolation phenomena of dielectric permittivity of a microwave-sintered $BaTiO_3$-Ag nanocomposite for high energy capacitor. *J. Alloys Compd.* 2020. **822**. P. 153525. https://doi.org/10.1016/j.jallcom.2019.153525.
44. Lunkenheimer P., Krohns S., Riegg S. *et al.* Colossal dielectric constants in transition-metal oxides. *Eur. Phys. J. Spec. Topics*. 2009. **180**. P. 61–89. https://doi.org/10.1140/epjst/e2010-01212-5.

45. Petzelt J., Nuzhnyy D., Bovtun V., Crandles D.A. Origin of the colossal permittivity of (Nb + In) co-doped rutile ceramics by wide-range dielectric spectroscopy. *Phase Trans.* 2018. **91**. P. 932. https://doi.org/10.1080/01411594.2018.1501801.
46. Rychetský I., Nuzhnyy D., Petzelt J. Giant permittivity effects from the core–shell structure modeling of the dielectric spectra. *Ferroelectrics*. 2020. **569**. P. 9. https://doi.org/10.1080/00150193.2020.1791659.
47. Morozovska A.N., Eliseev E.A., Chen D. *et al.* Building free energy functional from atomically-resolved imaging: atomic scale phenomena in La-doped $BiFeO_3$. *Phys. Rev. B*. 2019. **99**. P. 195440. https://doi.org/10.1103/PhysRevB.99.195440.
48. Heywang W. Semiconducting barium titanate. *J. Mater. Sci.* 1971. **6**. P. 1214. https://doi.org/10.1007/BF00550094.

Authors' contributions

O.S.P. and A.N.M. generated the research idea. O.S.P., V.O.K., V.V.V. and V.N.P. performed dielectric measurements and analyzed results. I.V.F. prepared the samples and characterized them. L.D.D. performed TEM analysis. and formulated the problem. E.A.E. performed numerical modeling and prepared corresponding figures. A.N.M. formulated the theoretical problem, performed analytical calculations, and analyzed results. A.N.M., V.O.K., and V.V.V. wrote the paper. V.N.P., E.A.E., and A.N.M. coordinated the research.

Authors and CV

Oleksandr S. Pylypchuk, PhD in Physics and Mathematics (Solid State Physics, 2015), Senior Researcher at the Department of Solid State Electronics, Institute of Physics. Author of more than 40 scientific publications. The area of his scientific interests includes transport properties of low-dimensional semiconductor structures and nanoscale materials.
E-mail: pylypchuk@iop.kiev.ua, https://orcid.org/0000-0003-0136-0799, https://www.scopus.com/authid/detail.uri?authorId=36640638100

Vladyslav O. Kolupaiev, graduated from Igor Sikorsky Kyiv Polytechnic Institute, National Technical University of Ukraine, with a Master's degree in Physics and Astronomy. Now a PhD student at the Institute of Physics, NAS of Ukraine. The current research interest is charge carrier transport phenomena and other properties of semiconductor nanoscale materials. E-mail: kolupaiev.v.o@gmail.com, https://orcid.org/0009-0006-5957-6735, https://www.scopus.com/authid/detail.uri?authorId=58799202200

Viktor V. Vainberg, Doctor of Sciences in Physics and Mathematics (Solid State Physics, 2015), Leading Researcher at the Department of Solid State Electronics, Institute of Physics. Author of more than 100 scientific publications. His current research trend is transport properties of low-dimensional semiconductor structures and nanoscale materials.
E-mail: viktor.vainberg@gmail.com, https://orcid.org/0000-0002-9840-8033, https://www.scopus.com/authid/detail.uri?authorId=56048664700

Vladimir N. Poroshin, Doctor of Sciences in Physics and Mathematics (2006), Deputy Director of Research, Institute of Physics, Head of the Department of Solid State Electronics. Authored more than 100 publications. The area of his scientific interests includes fundamental researches of the electron and phonon transport phenomena, magneto-transport of carriers in bulk semiconductors and quantum heterostructures, effects of absorption and emission of light by hot carriers in the terahertz range.
E-mail: poroshin@iop.kiev.ua, https://orcid.org/0000-0001-8217-3949, https://www.scopus.com/authid/detail.uri?authorId=7004252671

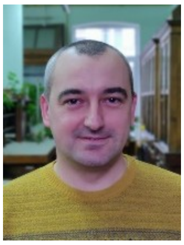

Ihor V. Fesych, PhD in Inorganic Chemistry (2012). Associate professsor at the Department of Inorganic Chemistry, Taras Shevchenko National University of Kyiv. Author of more than 55 scientific publications. The area of his scientific interests is sol-gel synthesis of oxide compounds and materials based on transition metal ions and rare earth elements with different dispersion, DTA/TG measurements, phase analysis, Rietveld refinement, and estimating average crystallite size using Williamson–Hall and Sherrer method. E-mail: ihor.fesych@knu.ua, https://orcid.org/0000-0002-4814-5642, https://www.scopus.com/authid/detail.uri?authorId=47061372300

Lesya Dmytrivna Demchenko, PhD in Metal Science and Thermal Treatment (1999), Associate Professor at the Department of Physical Material Science and Thermal Treatment, National Technical University of Ukraine "Igor Sikorsky Kyiv Polytechnic Institute". Author of more than 90 scientific publications. The area of her scientific interests is multifunctional nanomaterials, martensite transformations, shape memory alloys, nanomagnetism.
E-mail: lesyademch@gmail.com, https://orcid.org/0000-0002-2325-1940, https://www.scopus.com/authid/detail.uri?authorId=6506180411

Eugene A. Eliseev, PhD in Solid State Physics (2003), Doctor of Sciences in Solid State Physics (2009), Senior Researcher (2015), Head of the Department of Functional Oxide Materials, Department of Solid State Electronics, Institute of Physics. Author of more than 350 scientific publications. The area of his scientific interests is theory of ferroics and phase diagrams, mixed ionic-electronic conductors and related materials.
https://orcid.org/0000-0001-8124-8857, https://www.scopus.com/authid/detail.uri?authorId=6603821167

Anna N. Morozovska, PhD in Optics and Laser Physics (2004), Doctor of Sciences in Solid State Physics (2009), Professor in Physics and Astronomy (2023), Leading Scientific Researcher at the Department of Physics of Magnetic Phenomena at the Institute of Physics. Author of more than 400 scientific publications. The area of her scientific interests is theory of ferroics and multiferroics, mixed ionic-electronic conductors and related materials.
https://orcid.org/0000-0002-8505-458X, https://www.scopus.com/authid/detail.uri?authorId=6602682668

Кореляції між діелектричними властивостями, морфологією доменної структури та фазовим станом наночастинок $Bi_{1-x}Sm_xFeO_3$

О.С. Пилипчук, В.О. Колупаєв, В.В. Вайнберг, В.Н. Порошин, І.В. Фесич, Л.Д. Демченко, Е.А. Єлісєєв та А.Н. Морозовська

Анотація. Нанорозмірні мультифероїки є базовими модельними об'єктами для вивчення полярних, магнітних та магнітоелектричних властивостей і взаємних зв'язків. Ферит вісмут-самарію ($Bi_{1-x}Sm_xFeO_3$) є модельним ортоферитом, полярні, магнітні та магнітоелектричні властивості якого були досліджені для об'ємних та тонкоплівкових зразків. Властивості наночастинок $Bi_{1-x}Sm_xFeO_3$ були досліджені набагато менше, незважаючи на те, що наночастинки можуть бути використані в широкому спектрі застосувань, таких як накопичення енергії, магнітна гіпертермія та передова наноелектроніка. У цій роботі ми провели експериментальні вимірювання та аналіз температурної залежності діелектричних властивостей нанопорошків $Bi_{1-x}Sm_xFeO_3$. Розрахунки впливу фероіонного зв'язку на діелектричні властивості, морфологію доменної структури та фазові стани виконані в рамках підходу Гінзбурга–Ландау–Девоншира–Стефенсона–Хайленда. Теоретичні результати пояснюють основні тенденції експериментально спостережуваних температурних залежностей ефективної діелектричної проникності, що дозволяє зрозуміти кореляції між температурною поведінкою діелектричних властивостей, морфологією доменної структури та фазовим станом наночастинок $Bi_{1-x}Sm_xFeO_3$.

Ключові слова: мультифероїки, фероіонний зв'язок, діелектричні властивості, морфологія доменної структури, фазовий стан.